© 2022. Published by The Company of Biologists Ltd | Development (2022) 149, dev200458. doi:10.1242/dev.200458

RESEARCH ARTICLE

LONP1-mediated mitochondrial quality control safeguards metabolic shifts in heart development

Ke Zhao[1], Xinyi Huang[1], Wukui Zhao[1], Bin Lu[2] and Zhongzhou Yang[1,*]

ABSTRACT

The mitochondrial matrix AAA$^+$ Lon protease (LONP1) degrades misfolded or unassembled proteins, which play a pivotal role in mitochondrial quality control. During heart development, a metabolic shift from anaerobic glycolysis to mitochondrial oxidative phosphorylation takes place, which relies strongly on functional mitochondria. However, the relationship between the mitochondrial quality control machinery and metabolic shifts is elusive. Here, we interfered with mitochondrial quality control by inactivating *Lonp1* in murine embryonic cardiac tissue, resulting in severely impaired heart development, leading to embryonic lethality. Mitochondrial swelling, cristae loss and abnormal protein aggregates were evident in the mitochondria of *Lonp1*-deficient cardiomyocytes. Accordingly, the p-eIF2α-ATF4 pathway was triggered, and nuclear translocation of ATF4 was observed. We further demonstrated that ATF4 regulates the expression of *Tfam* negatively while promoting that of *Glut1*, which was responsible for the disruption of the metabolic shift to oxidative phosphorylation. In addition, elevated levels of reactive oxygen species were observed in *Lonp1*-deficient cardiomyocytes. This study revealed that LONP1 safeguards metabolic shifts in the developing heart by controlling mitochondrial protein quality, suggesting that disrupted mitochondrial quality control may cause prenatal cardiomyopathy.

KEY WORDS: LONP1, Mitochondrial quality control, ATF4, Glycolysis, Oxidative phosphorylation, Metabolic shift, Heart development, Mouse

INTRODUCTION

During mammalian embryogenesis, the heart is the first organ to develop and function (Olson and Srivastava, 1996; Harvey, 2002; Bruneau, 2020). Initially, heart tissues form under hypoxic conditions before embryonic day (E) 11.5, and hypoxia inducing factor α (HIFα) drives an anaerobic glycolysis program to provide energy through transcriptional mechanisms for early heart development (Guimarães-Camboa et al., 2015; Menendez-Montes et al., 2016; Maroli and Braun, 2021). From E11.5 onward, a metabolic shift from anaerobic glycolysis to mitochondrial oxidative phosphorylation (oxidative metabolism) takes place in cardiomyocytes, which is essential for myocardial development (Lopaschuk and Jaswal, 2010; Zhao et al., 2019; Maroli and Braun, 2021). Recently, we identified the chromatin-remodeling SRCAP complex as a pivotal regulator of mitochondrial oxidative metabolism for this type of metabolic shift/transition (Xu et al., 2021). Through transcriptional regulation, the SRCAP complex controls mitochondrial maturation morphologically and functionally to meet the energy requirements of the rapidly growing myocardium.

In the mitochondria, several distinct quality control machineries monitor the proteome, which contains ∼1500 proteins to safeguard mitochondrial functions (Fischer et al., 2012; Rugarli and Langer, 2012; Song et al., 2021). AAA$^+$ Lon protease (LONP1) is located in the mitochondrial matrix and functions to degrade misfolded proteins and prevent protein aggregation (Suzuki et al., 1994; Lu et al., 2013; Song et al., 2021). Under stress conditions, LONP1 can directly remove mitochondrial proteins, such as the components of the respiratory chain complexes and of the tricarboxylic acid (TCA) cycle, to sustain mitochondrial function (Song et al., 2021). There is also growing evidence to show that LONP1 acts as a chaperone to modulate mitochondrial DNA (mtDNA) stability (Chen et al., 2008; Matsushima et al., 2010; Kao et al., 2015). Thus, LONP1 plays a large role in governing mitochondrial protein folding and removing damaged proteins and, therefore, participates in mitochondrial quality control.

When cells are subjected to stresses, such as amino acid deprivation, viral infection, heme loss or endoplasmic reticulum (ER) stress, the integrated stress response (ISR) is elicited (Pakos-Zebrucka et al., 2016). Cellular stresses provoke a remarkable elevation in phosphorylated eukaryotic initiation factor 2α (*P*-eIF2α), further leading to an increase in translation of the master regulator of ISR, activating transcription factor 4 (ATF4) (Jousse et al., 2003; Lu et al., 2004; Dara et al., 2011). ATF4 stimulates a transcriptional program to regulate protein synthesis, the unfolded protein response (UPR), autophagy and metabolism (Vattem and Wek, 2004; Kilberg et al., 2009; B'Chir et al., 2013). A recent study indicated that mitochondrial morphological damage and/or dysfunction gives rise to mitochondrial stress and causes the accumulation of ATF4 (Quirós et al., 2017). Mitochondrial stress also promotes the decreased expression of mitochondrial ribosomal proteins (MRPs) to attenuate protein translation (Quirós et al., 2017).

Global deletion of *Lonp1* in mice causes embryonic lethality at E8.5, and knockout embryos exhibit a decline in mtDNA copy number (Quiros et al., 2014). To address whether mitochondrial quality control plays a role in organogenesis and in the surveillance of mitochondrial metabolic shifts, we knocked out *Lonp1* in embryonic cardiac tissues. *Lonp1* deficiency caused severely defective heart development and embryonic lethality. Aggregates were evident in the mitochondria of *Lonp1*-deficient cardiomyocytes. Accordingly, AFT4 accumulation was shown to not only suppress the expression of *Tfam*- and mtDNA-encoded components of respiratory chain complexes, but also enhance the expression of

[1]State Key Laboratory of Pharmaceutical Biotechnology, MOE Key Laboratory of Model Animal for Disease Study, Model Animal Research Center, and Jiangsu Key Laboratory of Molecular Medicine, Nanjing University Medical School, Nanjing 210093, China. [2]Department of Biochemistry and Molecular Biology, School of Basic Medical Sciences, Hengyang Medical School, University of South China, Hengyang, Hunan 421001, China.

*Author for correspondence (zhongzhouyang@nju.edu.cn; lubinmito@usc.edu.cn)

Z.Y., 0000-0002-3272-5255

Handling Editor: Benoit Bruneau
Received 13 December 2021; Accepted 13 February 2022

Development (2022) 149, dev200458. doi:10.1242/dev.200458

glycolysis regulatory genes, including *Glut1* (*Slc2a1*) resulting in a disrupted metabolic shift during cardiac development.

RESULTS

Lonp1 deficiency in cardiac progenitors impairs ventricular development

We examined the level of LONP1 protein in the developing heart tissue at different developmental stages, and found a slight, but significant, enhancement from E10.5 to E12.5 (Fig. S1A,B). During this period, the anaerobic glycolysis regulatory protein GLUT1 was significantly reduced and had almost disappeared by E12.5 (Fig. S1A). By contrast, the mitochondrial oxidative metabolic protein NDUFB8, a component of respiratory chain complex I (CI), was significantly increased (Fig. S1A). These results indicate a metabolic shift from anaerobic glycolysis to mitochondrial oxidative phosphorylation from E10.5 to E13.5 and suggest that LONP1 may be involved.

To determine whether LONP1 is involved in heart development, we first deleted *Lonp1* in the cardiac progenitors of the second heart field, which contributes to the development of the cardiac outflow tract (OFT) and the right ventricle (RV). *Lonp1*-deficient mice (*Mef2c-AHF-Cre; Lonp1*$^{F/F}$) showed comparable heart morphology with the control at E9.5 (Fig. 1A-A″), and ISL1 staining for cardiac progenitors revealed a normal distribution of progenitor cells (Fig. 1B). Furthermore, we observed normal OFT morphogenesis and septation (Fig. S2). Thus, *Lonp1* deficiency does not affect cardiac progenitor development.

However, *Lonp1*-deficient mice showed reduced RV size from E11.5 onward, and RV hypoplasia was more prominent from E12.5 to E18.5 (Fig. 1C,D). Interestingly, *Lonp1*-deficient mice showed increased LV size from E14.5 onward (Fig. 1E). Although *Lonp1*-deficient mice were viable at birth, all were lost by postnatal day (P) 0. The hearts of *Lonp1*-deficient mice showed enlargement of the two atria and a small RV at birth, indicating heart failure (Fig. 1F-F″).

TUNEL staining to detect cell death showed no obvious apoptosis signals in *Mef2c-AHF-Cre; Lonp1*$^{F/F}$ hearts (Fig. 1G-G″). In contrast, knockout of *Lonp1* led to a significant decrease in cardiac cell proliferation (Fig. 1H). Further study revealed that the cells with reduced proliferation were primarily cardiomyocytes (Fig. 1I).

Thus, overall, deletion of *Lonp1* has little effect on cardiac progenitor development but impairs cardiomyocyte proliferation in the RV.

Deletion of *Lonp1* in cardiomyocytes results in poorly developed myocardium

Lonp1 deletion in cardiac progenitors impeded cardiomyocyte proliferation in the RV. To confirm this phenotype, we deleted *Lonp1* in embryonic cardiomyocytes using *cTnT-Cre* mice to generate *cTnT-Cre; Lonp1*$^{F/F}$ mice (cardiomyocyte-specific *Lonp1*-deficient mice). Similar to *Lonp1* deletion in cardiac progenitors, there was no significant change in OFT development or progenitor cell contribution in the hearts of cardiomyocyte-specific *Lonp1*-deficient mice (Fig. 2A,B). However, these mice started to demonstrate reduced ventricular volume from E11.5 and a thinned ventricular wall at E14.5 (Fig. 2C-E) and did not survive after E16.5 (Fig. 2F). The TUNEL assay did not reveal an increase in apoptotic cardiomyocytes (Fig. 2G). However, a cell proliferation analysis indicated significantly reduced cardiomyocyte proliferation during an early stage of cardiac development (Fig. 2H-H″). These results confirm the essential role of LONP1 in embryonic cardiomyocyte development.

Lonp1 deficiency causes mitochondrial abnormalities, increased ROS production and DNA damage

LONP1 is primarily located in the mitochondrial matrix. To determine whether deletion of *Lonp1* affects mitochondrial morphology, we isolated cardiomyocytes from the hearts of control and *cTnT-Cre; Lonp1*$^{F/F}$ mice and cultured them *in vitro*. We then examined the mitochondria and found a dramatic morphological difference between control and *Lonp1*-deficient cardiomyocytes. Whereas the mitochondria in control cardiomyocytes showed a slender lamellar network, those in *Lonp1*-deficient cardiomyocytes contained aggregated lamellar structures (Fig. S3). Next, we performed transmission electron microscopy (TEM) analysis to study the mitochondria in the hearts of control and *Lonp1*-deficient mice. The results showed accumulation of highly electron-dense substances in the cardiomyocytes from *cTnT-Cre; Lonp1*$^{F/F}$ mice (Fig. 3A-F). In addition, mitochondria in these cardiomyocytes were swollen and cristae could not be seen (Fig. 3D-F). Compared with the control group, the damage to mitochondria increased significantly in cardiomyocytes from *cTnT-Cre; Lonp1*$^{F/F}$ mice [Fig. 3G; Ctrl: 0.01167±0.008731 versus conditional knockout (cKO): 0.1947±0.04107].

Severe mitochondrial abnormalities could trigger the increased production of reactive oxygen species (ROS). Significantly increased levels of ROS were observed in *Lonp1*-deficient cardiomyocytes (Fig. 3H-H″,I). High levels of ROS suppress cell cycle progression, and we found that the mRNA levels of *Cdkn1a* and *Ddit3* were significantly increased in cKO hearts (Fig. 3J), suggesting inhibition of the cell cycle. In addition, we observed a significantly increased level of γH2A.X, a DNA damage marker in *Lonp1*-deficient cardiomyocytes (Fig. 3K,L).

Taken together, these results demonstrate that *Lonp1* deletion causes mitochondrial abnormalities, increased ROS production and DNA damage.

Altered metabolic pattern in the *Lonp1*-deficient heart

Deletion of *Lonp1* impaired heart development starting at E11.5 (Fig. 2C), a developmental stage at which a metabolic shift takes place from anaerobic glycolysis to mitochondrial oxidative phosphorylation. To determine whether *Lonp1* deficiency affects this metabolic shift, we examined the metabolic pattern in the hearts of control and *Lonp1*-deficient mice. Western blot analysis showed that protein levels of the CI component NDUFB8 and the complex IV (CIV) component mitochondrial (mt)-COX2 were reduced significantly compared with those of the control as early as E11.5 (Fig. S4A,B). At E12.5, the protein levels of the CIV component COX4 and the complex V (CV) component ATP5a1 were substantially decreased compared with those of the control (Fig. 4A,B). Immunofluorescence (IF) staining also confirmed a significant reduction in NDUFB8 in *Lonp1*-deficient cardiomyocytes (Fig. S4C).

In contrast, we observed markedly enhanced protein levels of GLUT1 and GLUT4 in the hearts of *Lonp1*-deficient mice (Fig. 4C-E; Fig. S4D). In addition, the transcript levels of *Glut1*, *Glut4* (*Slc2a4*) and *Hk2* were also elevated in a HIF1-independent manner in the hearts of *Lonp1*-deficient mice compared with control mice (Fig. S4E-I). Phosphorylation of AMPK can represent the tissue energy balance; we found a substantial increase in phosphor-AMPK levels in the *Lonp1*-deficient hearts compared with control hearts, indicating an energy shortage (Fig. 4F,G).

Taken together, these results demonstrate that a relatively high level of glycolysis takes place in the *Lonp1*-deficient heart, suggesting a disrupted metabolic shift.

Development (2022) 149, dev200458. doi:10.1242/dev.200458

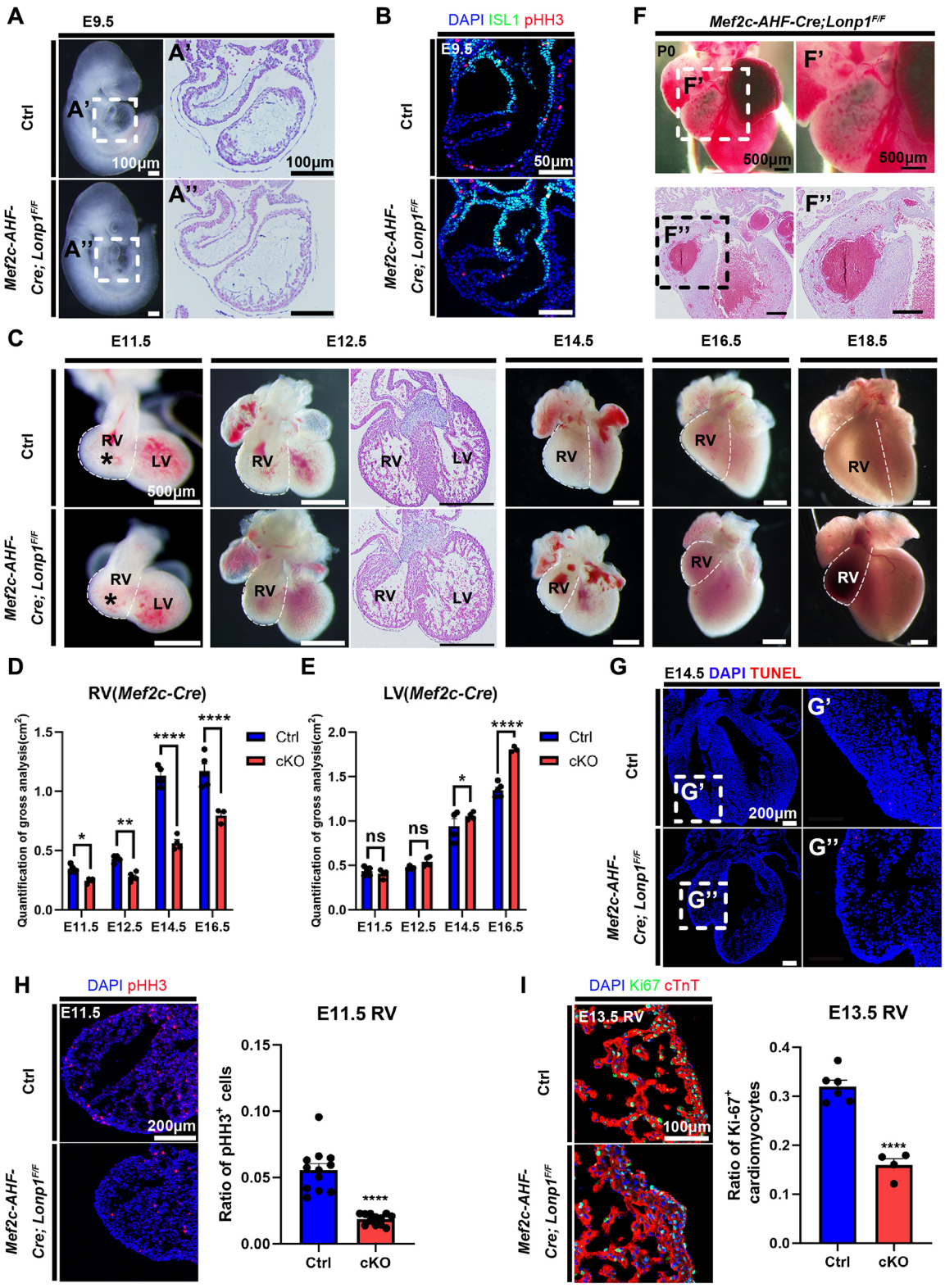

Fig. 1. Deletion of *Lonp1* in cardiac progenitors causes right ventricle hypoplasia. (A-A″) Gross analysis of embryos and H&E staining (A′,A″) of heart tissues at E9.5 in control and *Lonp1*-deficient mice (*n*=5). (B) Cell proliferation and ISL1$^+$ progenitor cell distribution (*n*=3) in control and *Lonp1*-deficient mice. (C) Gross analysis of hearts at different embryonic stages and H&E staining of hearts at E12.5 in control and *Lonp1*-deficient mice (*n*=3-5). Asterisks indicate a reduction in right ventricle (RV) volume starting at E11.5. The dotted line outlines the RV. (D,E) Quantification of RV (D) and left ventricle (LV) (E) in C (*n*=3-5). cKO indicates *Lonp1*-deficient mice. (F-F″) Gross analysis and H&E staining of *Lonp1*-deficient hearts at P0. (G-G″) TUNEL staining of the two ventricles at E14.5 in control and *Lonp1*-deficient mice. (H) Cell proliferation analysis and quantification of the RV at E11.5 in control and *Lonp1*-deficient mice (*n*=12). (I) Cardiomyocyte proliferation analysis and quantification of RV at E13.5 in control and *Lonp1*-deficient mice (*n*=6 versus 4). Proliferating cells are labeled with pHH3 and Ki-67 antibodies. Cardiomyocytes are marked by cTnT. Data are mean±s.e.m. **P*<0.05, ***P*<0.01, *****P*<0.0001, ns, not significant on two-tailed unpaired Student's *t*-test.

Development (2022) 149, dev200458. doi:10.1242/dev.200458

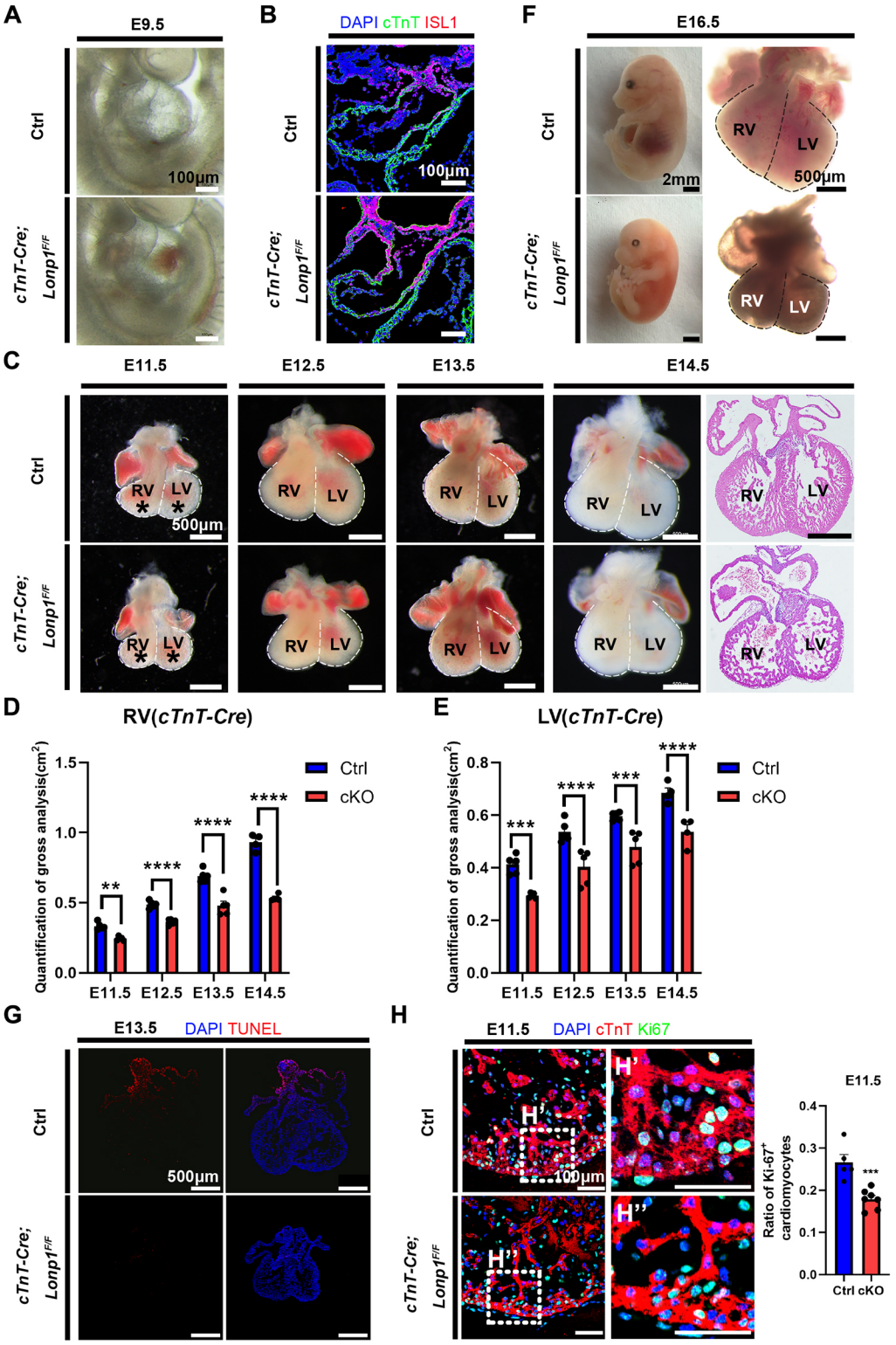

Fig. 2. *Lonp1* deficiency in embryonic cardiomyocytes impairs myocardial development. (A) Gross analysis of control and *Lonp1*-deficient embryos at E9.5 (n=3). (B) ISL1$^+$ progenitor cell distribution. (C) Gross analysis of hearts at different embryonic stages and H&E staining of heart tissues at E14.5 in control and *Lonp1*-deficient embryos. Asterisks indicate a reduction in ventricular volume starting at E11.5. The dotted line outlines the two ventricles. (D,E) Quantification of right ventricle (RV; D) and left ventricle (LV; E) areas of C (n=4 or 5). (F) Gross analysis of control and *Lonp1*-deficient embryos (left) and hearts (right) at E16.5. The dotted lines outline the two ventricles. All *Lonp1*-deficient embryos died after E16.5 (n=4-6). (G) TUNEL staining of ventricles at E13.5 in control and *Lonp1*-deficient hearts. (H-H″) Cell proliferation analysis of cardiomyocytes and quantification at E11.5 in control and *Lonp1*-deficient hearts (n=5 versus 7, respectively). Proliferating cells are labeled with Ki-67 antibody. Data are mean±s.e.m. $^{**}P$<0.01, $^{***}P$<0.001, $^{****}P$<0.0001 on two-tailed unpaired Student's t-test.

Lonp1 deficiency activates ATF4 expression

We performed RNA-sequencing (RNA-seq) using RNA isolated from control and *Lonp1*-deficient heart tissues. By comprehensive alignment analysis of the altered genes and Gene Ontology (GO) analysis, we found that *Atf4* was highly expressed in *Lonp1*-deficient hearts (Fig. 5A). Quantitative real-time PCR analysis confirmed significantly elevated mRNA levels of *Atf4* in *Lonp1*-deficient hearts compared with control hearts at both E10.5 and E12.5 (Fig. 5B). Western blot analysis also showed a marked increase in AFT4 levels in *Lonp1*-deficient hearts (Fig. 5C,D). IF staining clearly showed increased expression of ATF4 in both the nucleus and cytoplasm from E10.5 to E12.5 (Fig. 5E; Fig. S5A). Accordingly, there was significantly increased expression of the downstream target genes of ATF4 (*Pck2*, *Phgdh*, *Shmt2*, *Pc*, etc.) (Fig. S5B-D). In addition, there were elevated phosphorylation levels of eIF2α in *Lonp1*-deficient hearts (Fig. 5F,G).

Development (2022) 149, dev200458. doi:10.1242/dev.200458

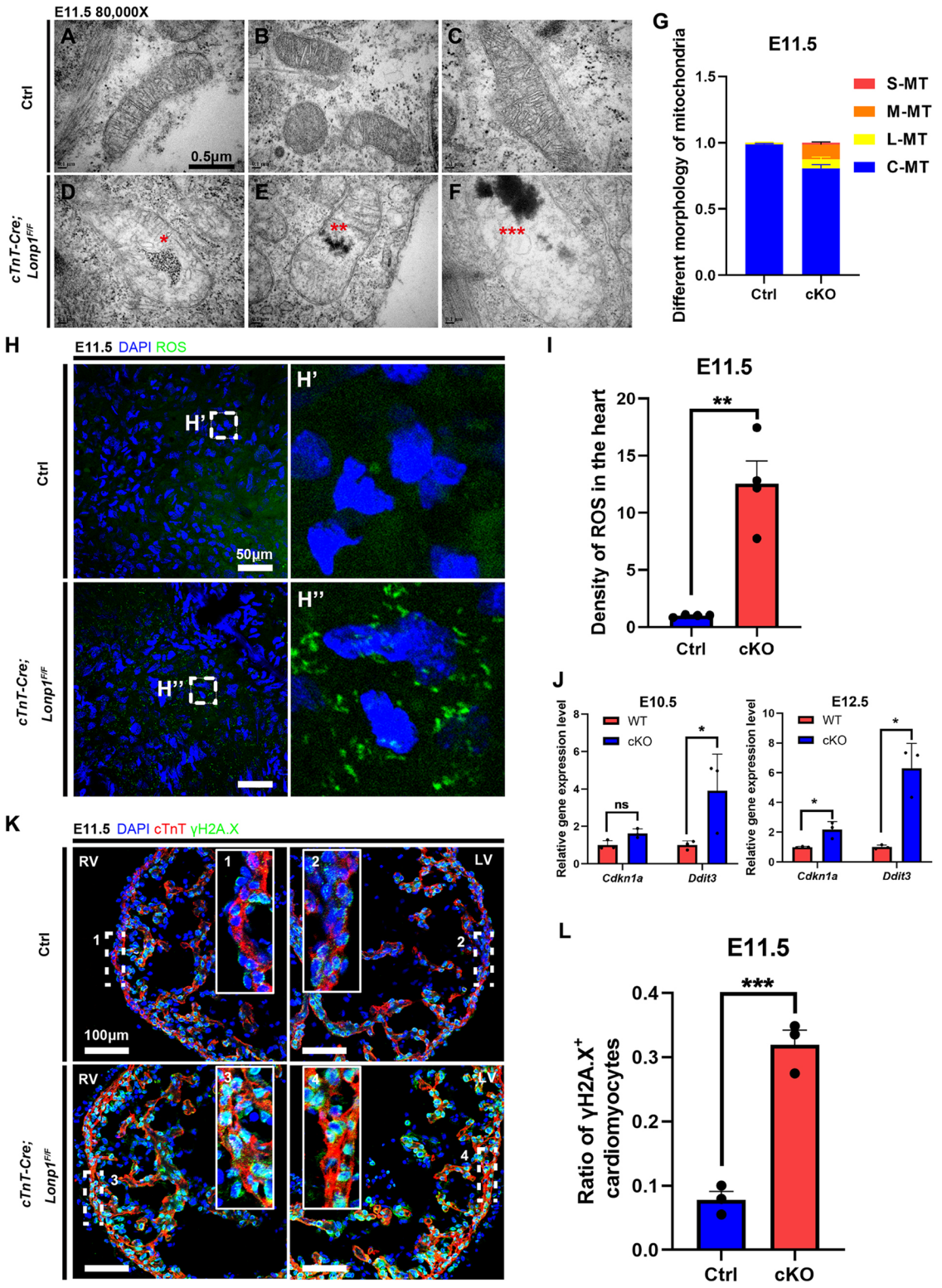

Fig. 3. *Lonp1* deficiency causes mitochondrial abnormalities, increased ROS production and DNA damage. (A-F) TEM images of mitochondria in control and *Lonp1*-deficient cardiomyocytes at E11.5. Control groups (A-C) have normal mitochondria, whereas *Lonp1*-deficient groups (D-F) show accumulation of aggregates, mitochondrial swelling and disappearance of mitochondrial cristae (red asterisks). (G) Quantification of different mitochondria morphologies. C-MT indicates complete mitochondria; L-MT indicates lightly damaged mitochondria, as represented in D; M-MT indicates moderately damaged mitochondria, as represented in E; S-MT indicates severely damaged mitochondria, as represented in F (n=3). cKO indicates *cTnT-Cre; Lonp1*$^{F/F}$ cardiomyocytes. (H-H″) Oxidized H2DCF (green) indicates an increase in ROS levels in the hearts of *Lonp1*-deficient mice. (I) Quantification of ROS density in the heart at E11.5 (n=4). (J) Expression level of genes associated with cell cycle inhibition in E10.5 and E12.5 hearts (n=3). (K) Increased level of γH2A.X, a DNA damage marker, in *Lonp1*-deficient cardiomyocytes (n=3). Numbered panels show the dashed boxes at higher magnification. (L) Quantification of images in K. Data are mean±s.e.m. *P<0.05, **P<0.01, ***P<0.001, ns, not significant on two-tailed unpaired Student's t-test.

Development (2022) 149, dev200458. doi:10.1242/dev.200458

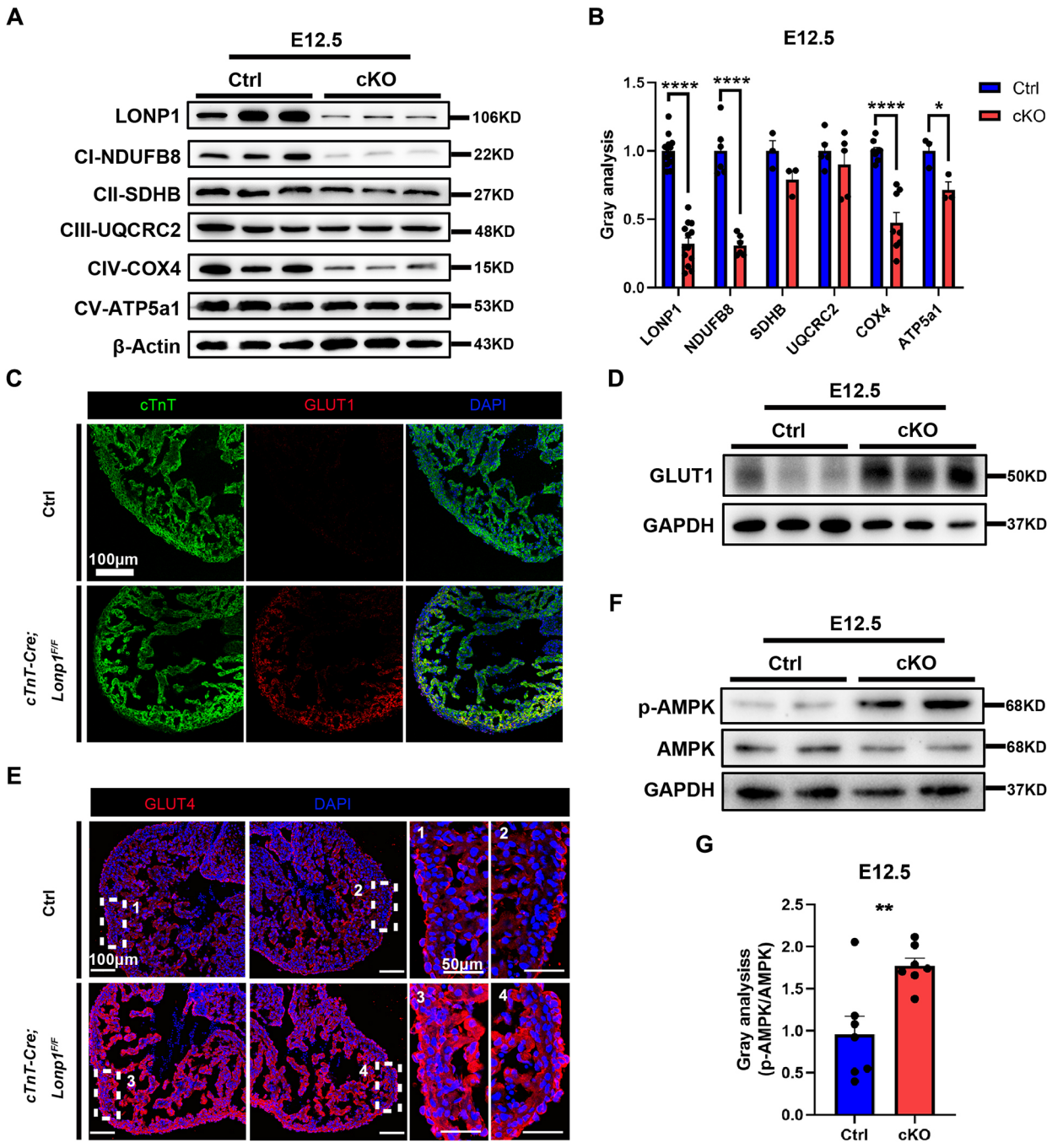

Fig. 4. Altered metabolic pattern in *Lonp1*-deficient hearts. (A,B) Western blot analysis (A) and quantification (B) of components of respiratory chain complexes in E12.5 control and *cTnT-Cre; Lonp1*$^{F/F}$ (cKO) hearts (n=3-12). (C) Increased GLUT1 levels in control and cKO ventricles (n=3). (D) Western blot analysis of GLUT1 in E12.5 control and cKO hearts (n=6). (E) Increased GLUT4 levels in control and cKO ventricles (n=3). Right panels show the numbered dashed boxes at higher magnification. (F,G) Western blot analysis (F) and quantification (G) of p-AMPK in E12.5 control and cKO hearts (n=7). Data are mean±s.e.m. *P<0.05, **P<0.01, ****P<0.0001 on two-tailed unpaired Student's t-test.

Collectively, these results demonstrate a substantial increase in ATF4 levels and suggest that this is related to elevated phosphorylation of eIF2α.

Reduced protein levels of TFAM and mtDNA-encoded components of respiratory chain complexes in *Lonp1*-deficient hearts

Mitochondrial respiratory chain complex components are coordinately encoded by nuclear DNA and mtDNA. Gene expression analysis revealed no significant change in the mRNA levels of mitochondrial respiratory chain complex components encoded by nuclear DNA (Fig. 6A). However, the mRNA levels of respiratory chain complex components encoded by mtDNA (*mt-Cox2* and *mt-Atp6*) were significantly decreased in *Lonp1*-deficient hearts compared with control hearts (Fig. 6A; Fig. S6A). A previous study detected a decreased mtDNA copy number in global *Lonp1*-deficient mice (Quiros et al., 2014). In the current study, there was a substantial reduction in the total amount of mtDNA in *Lonp1*-deficient hearts (Fig. 6B). As the most abundant mtDNA-binding protein, mitochondria-associated transcription factor A

Development (2022) 149, dev200458. doi:10.1242/dev.200458

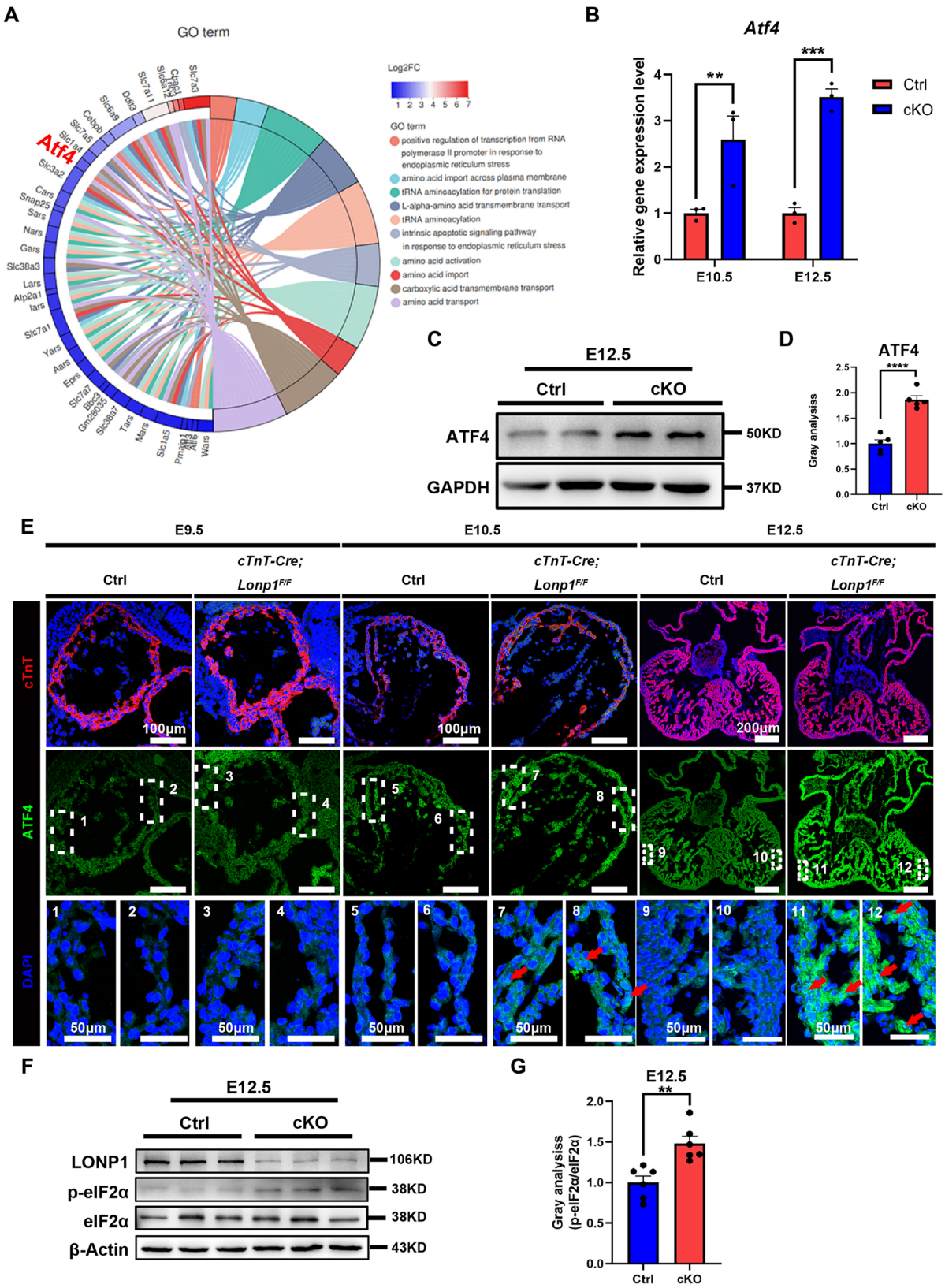

Fig. 5. Enhanced ATF4 levels in *Lonp1*-deficient hearts. (A) Comprehensive alignment of the altered genes (left) and GO analysis (right) in *Lonp1*-defiicent hearts. ATF4 is highlighted. (B) Expression of *Atf4* in E10.5 and E12.5 control (Ctrl) and *cTnT-Cre; Lonp1*$^{F/F}$ (cKO) hearts (n=3). (C,D) Western blot analysis (C) and quantification (D) of ATF4 in E12.5 control and cKO hearts (n=5). (E) Level of ATF4 gradually increases with *Lonp1*-deficient cardiac development. The red arrows indicate ATF4 co-located with DAPI. Bottom panels show the numbered dashed boxes at higher magnification (n=3). (F,G) Western blot analysis (F) and quantification (G) of p-eIF2α in E12.5 control and cKO hearts (n=6). Data are mean±s.e.m. **P<0.01, ***P<0.001, ****P<0.0001 on two-tailed unpaired Student's t-test.

Development (2022) 149, dev200458. doi:10.1242/dev.200458

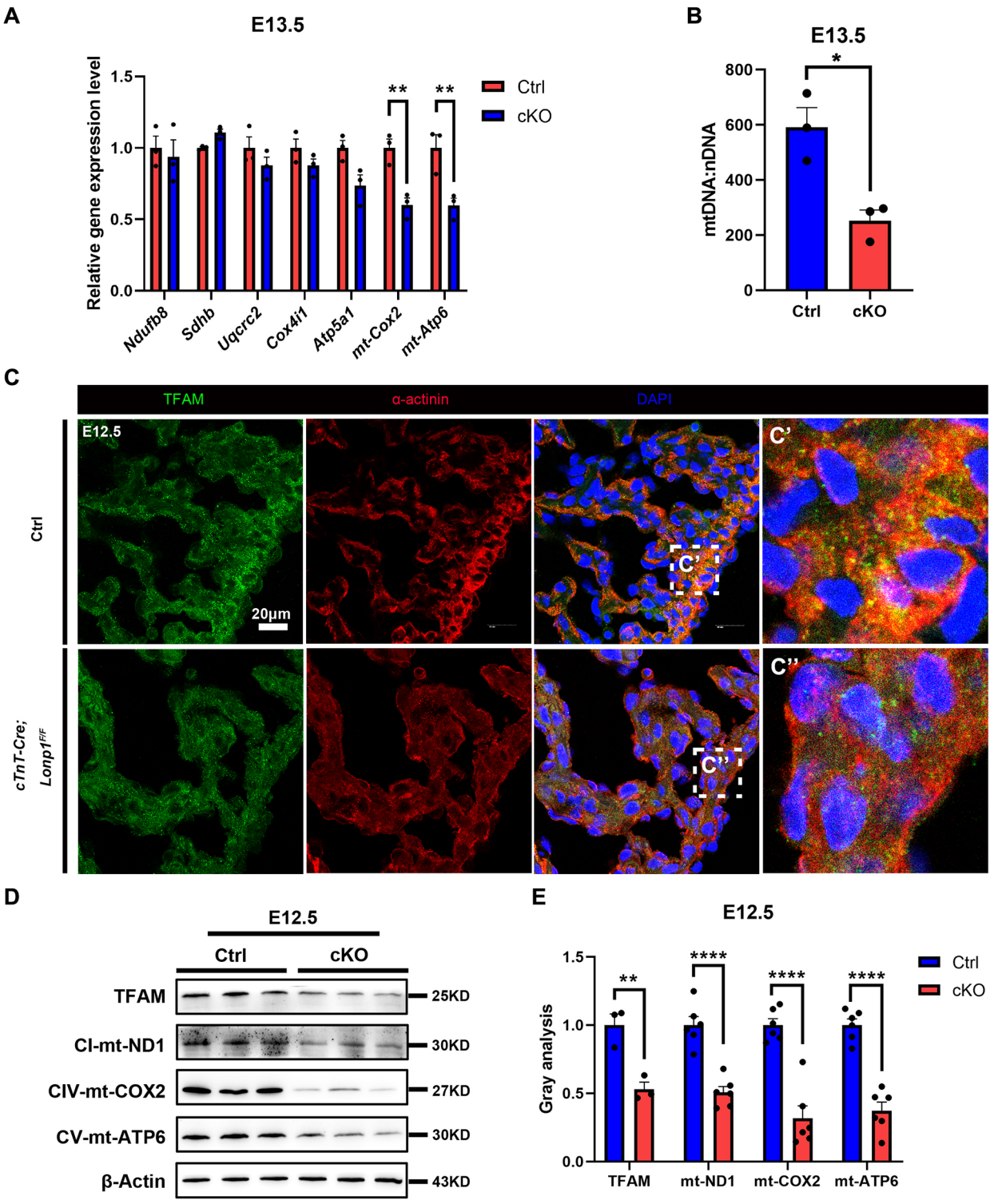

Fig. 6. *Lonp1* deficiency reduces the levels of TFAM, mtDNA and mtDNA-encoded respiratory chain complex components. (A) Expression of nuclear DNA and mtDNA genes encoding respiratory chain complex components in E13.5 control (Ctrl) and *cTnT-Cre; Lonp1*$^{F/F}$ (cKO) hearts (*n*=3). (B) mtDNA copy number in E13.5 hearts (*n*=3). (C-C″) Decrease in TFAM levels in *Lonp1*-deficient hearts compared with control hearts (*n*=3). (D,E) Western blot analysis (D) and quantification (E) of TFAM- and mtDNA-encoded respiratory chain complex components in E12.5 control and cKO hearts (*n*=3-6). Data are mean±s.e.m. **P*<0.05, ***P*<0.01, *****P*<0.0001 on two-tailed unpaired Student's *t*-test.

(TFAM) regulates mtDNA replication and transcription (Matsushima et al., 2010). Examination of the level of TFAM showed a profound decrease in *Lonp1*-deficient hearts (Fig. 6C-C″,D). Accordingly, the protein levels of mtDNA-encoded CI ND1 (CI-mt-ND1), CIV-mt-COX2 and CV-mt-ATP6 were all significantly decreased in *Lonp1*-deficient hearts compared with control hearts (Fig. 6D,E).

Furthermore, reductions in TFAM and mtDNA-encoded respiratory chain complex components in the *Lonp1*-deficient heart occurred at E11.5 rather than at E10.5 (Fig. S6B-E).

Development (2022) 149, dev200458. doi:10.1242/dev.200458

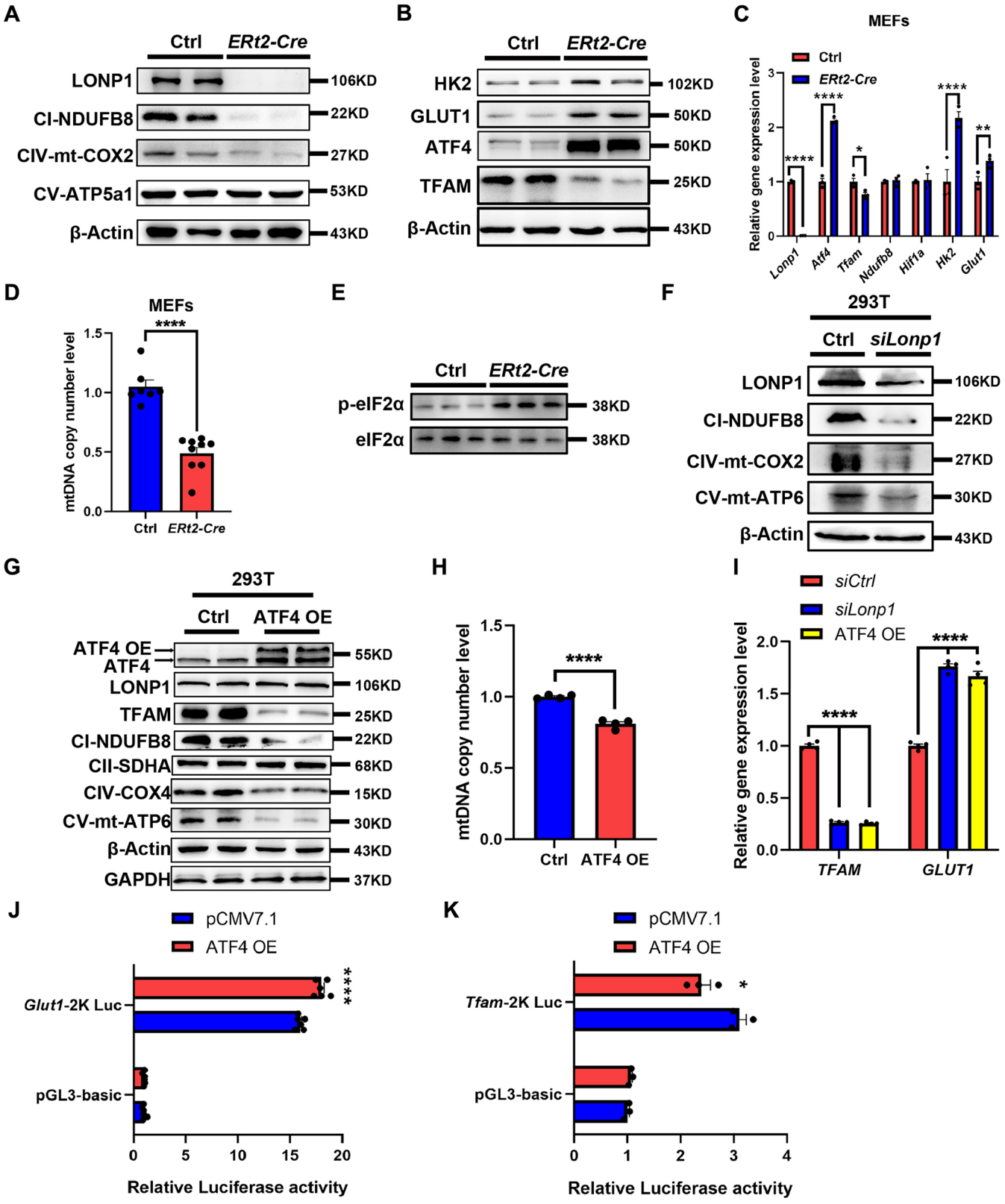

Fig. 7. ATF4 directly regulates *Tfam* and *Glut1* transcription. (A) Western blot analysis of respiratory chain complex components in MEFs. *ERt2-Cre* indicates *ERt2-Cre; Lonp1*$^{F/F}$+4-OH Tamoxifen MEFs (*n*=3-6). (B) Western blot analysis of MEFs (*n*=3-6). (C) Gene expression study of control versus *ERt2-Cre* MEFs (*n*=3). (D) mtDNA copy number in control versus *ERt2-Cre* MEFs (*n*=7 versus 9). (E) Western blot analysis of p-eIF2α in control versus *ERt2-Cre* MEFs (*n*=3). (F) Western blot analysis of respiratory chain complex components in 293T cells (*n*=3-6). *siLonp1* indicates *Lonp1* knockdown. (G) Western blot analysis of 293T cells (*n*=5 or 6). (H) mtDNA copy number in control and ATF4 OE 293T cells (*n*=4). (I) Expression of *Tfam* and *Glut1* in control, *siLonp1* and ATF4-OE 293T cells (*n*=4). (J,K) ATF4 activates the promoter activity of *Glut1* (J) but represses the promoter activity of *Tfam* (K) (*n*=6 and 3). Data are mean±s.e.m. **P*<0.05, ***P*<0.01, *****P*<0.0001 on two-tailed unpaired Student's *t*-test or two-way ANOVA.

Development (2022) 149, dev200458. doi:10.1242/dev.200458

Thus, *Lonp1* deficiency results in reduced protein levels of TFAM and mtDNA-encoded components of respiratory chain complexes.

ATF4 suppresses the expression of *Tfam* but promotes that of *Glut1*

Next, we constructed inducible *Lonp1*-deficient mouse embryonic fibroblasts (MEFs) derived from *ERt2; Lonp1*$^{F/F}$ mice. Upon 4-OH tamoxifen administration, MEFs without *Lonp1* showed abnormal mitochondrial morphological alterations (Fig. S7A), which was consistent with the results in *Lonp1*-deficient cardiomyocytes (Fig. S3). MEFs lacking *Lonp1* also showed a decrease in the expression level of respiratory chain complex components CI-NDUFB8 and CIV-mt-COX2 but an increase in glycolysis regulatory proteins (Fig. 7A,B). In addition, there was an increase in ATF4 protein levels and a decrease in TFAM protein levels in MEFs lacking *Lonp1* (Fig. 7B). Quantitative real-time PCR results showed that the changes in the transcription levels of these genes were consistent with those in *Lonp1*-deficient hearts (Fig. 7C). Accordingly, decreased mtDNA copy number was also observed in *Lonp1*-deficient MEFs (Fig. 7D), whereas the p-eIF2α level was enhanced in *Lonp1*-deficient MEFs (Fig. 7E). Similar alterations were observed in human 293T cells (Fig. 7F) and rat H9C2 cells (Fig. S7B), suggesting conserved regulation across species and cell types.

Furthermore, we overexpressed ATF4 (ATF4 OE) in several cell lines. This did not affect the expression level of LONP1 but was sufficient to reduce that of TFAM (Fig. 7G; Fig. S7C) and led to decreased levels of respiratory chain complex components (Fig. 7G). Accordingly, the ATF4 OE groups showed a lower mtDNA copy number (Fig. 7H). In addition, there was a decrease in the *Tfam* transcription level but an increase in the *Glut1* transcription level in *Lonp1*-knockdown cells and ATF4 OE cells (Fig. 7I). ATF4 positively or negatively regulates target gene expression by binding to the cAMP response element (CRE) sequences proximal to the promoter regions of the target gene (Koyanagi et al., 2011). We identified the CRE sequences in the promoters of both *Tfam* and *Glut1* and constructed luciferase reporters. A luciferase reporter assay revealed that ATF4 activated the promoter activity of *Glut1* but repressed the promoter activity of *Tfam* (Fig. 7J,K). Collectively, these results demonstrate that ATF4 directly represses the transcription of *Tfam* but activates the transcription of *Glut1*.

Pharmacological inhibition of LONP1 activates ATF4

To further understand the relationship between *Lonp1* deficiency and AFT4 activation, we administered CDDO, a well-established LONP1 inhibitor, to cells to mimic *Lonp1* deletion (Bernstein et al., 2012; Zurita Rendon and Shoubridge, 2018; Shin et al., 2021). We first tested the dosage effect of CDDO on cell proliferation and found that, at doses ranging from 1.5 to 2.5 µM, CDDO significantly decreased the proliferative capacity of the cells (Fig. S8A-C); CDDO treatment also substantially reduced the protein levels of respiratory chain complex components (Fig. 8A; Fig. S8D). We also observed the time course-dependent accumulation of ATF4 but a reduction in TFAM, CIV-COX4 and CV-mt-APT6 (Fig. 8B). Treatment of cells with CDDO (2.5 µM) for 10 h substantially enhanced the mRNA and protein levels of ATF4 but remarkably decreased the mRNA levels of *Tfam* (Fig. 8C-E). CDDO administration was also sufficient to change the mitochondrial morphology and to augment the level of ROS (Fig. S8E).

DISCUSSION

Although mitochondrial abnormalities can cause heart developmental defects, the importance of mitochondrial quality

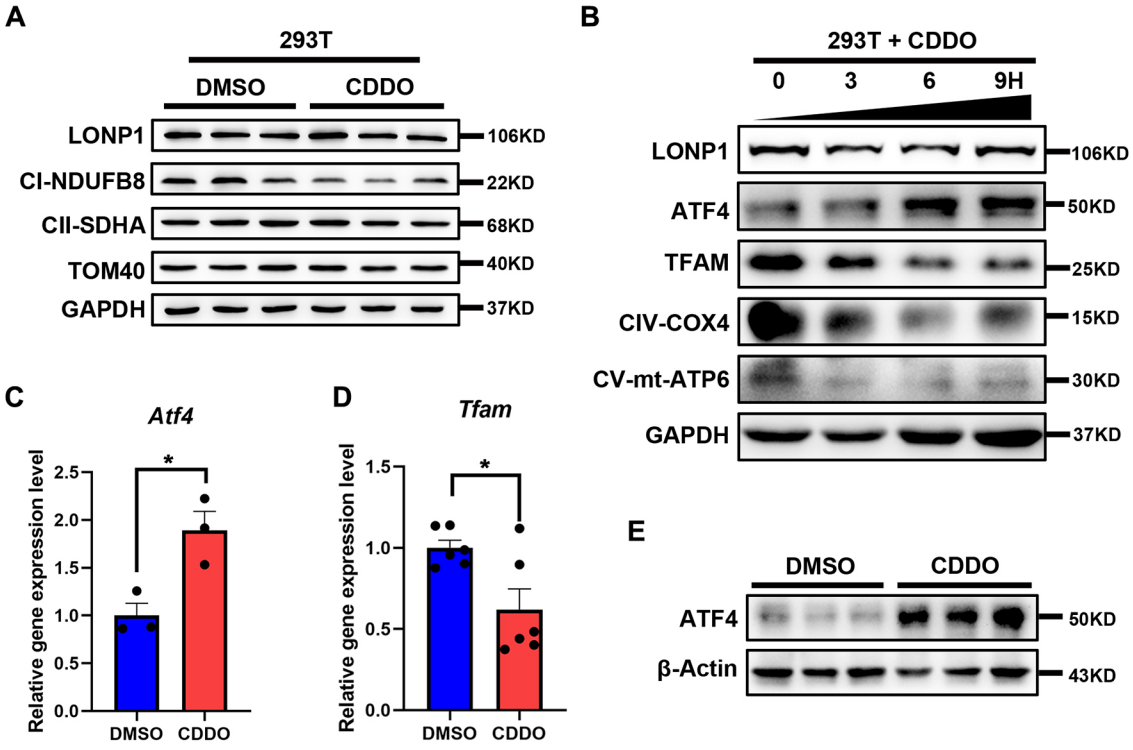

Fig. 8. CDDO treatment mimics *Lonp1* deficiency. (A) Western blot analysis of respiratory chain complex components in 293T cells treated with 2.5 µM CDDO for 10 h (*n*=3). (B) Western blot analysis in 293T cells treated with 2.5 µM CDDO (*n*=3). (C,D) Expression of *Atf4* (C) and *Tfam* (D) in 293T cells treated with DMSO or 2.5 µM CDDO (10 h, *n*=3 and 6, respectively). (E) Western blot analysis of ATF4 (*n*=3). Data are mean±s.e.m. **P*<0.05 on two-tailed unpaired Student's *t*-test.

Development (2022) 149, dev200458. doi:10.1242/dev.200458

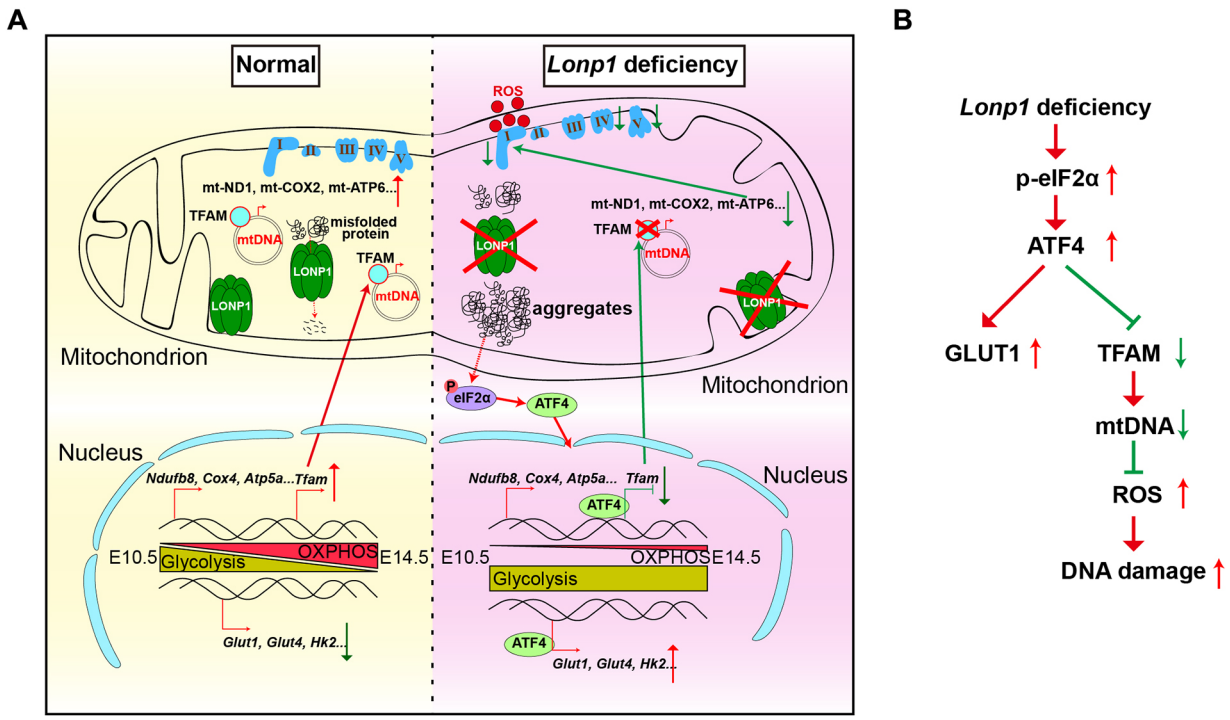

Fig. 9. Working model of embryonic cardiac development and the impact of *Lonp1* deficiency. (A) Under normal conditions (left), a metabolic shift from anaerobic glycolysis to oxidative phosphorylation takes place at approximately E10.5. LONP1 degrades misfolded or oxidized proteins to safeguard the metabolic shift and cardiac development. In the absence of *Lonp1* (right), misfolded or oxidized proteins form aggregates, which activate the p-eIF2α-ATF4 signaling pathway. Subsequently, ATF4 promotes *Glut1* expression but represses *Tfam* expression by directly binding to their promoters. Decreased TFAM levels reduce the amount and transcription of mtDNA, affecting the assembly of respiratory chain complexes. Mitochondrial dysfunction generates a large amount of ROS, which causes DNA damage and inhibits cell proliferation. (B) Red arrows indicate increases, and green arrows indicate decreases, in levels and/or activities of the indicated players in response to *Lonp1* deficiency.

control for prenatal heart development has not been well documented. Our study shows that the mitochondrial matrix protease LONP1, as a key element in controlling mitochondrial quality control, has a crucial role in embryonic heart development. In combination with mouse genetics and pharmacological treatment, we demonstrated that LONP1-mediated mitochondrial quality control safeguarded the metabolic shift during heart development to meet the energy demands of the growing myocardium and embryonic body.

We identified AFT4 as an important mediator of abolished mitochondrial quality control. Disruption of mitochondrial quality control resulted in a profound accumulation of ATF4, probably as a consequence of activation of the ISR-p-eIF2α signaling pathway, which is consistent with the results of a previous study (Quirós et al., 2017).

We also determined that *Tfam* is a pivotal target gene of ATF4. A CRE was discovered in the promoter region of *Tfam*, and a biochemical study demonstrated that ATF4 negatively regulates *Tfam* transcription. Consequently, the expression of several mtDNA-encoded respiratory chain complex components was significantly suppressed after ATF4 activation, which in turn hindered mitochondrial oxidative metabolism. In addition, we found that the key anaerobic glycolysis gene *Glut1* is another target gene of ATF4. Through direct regulation, ATF4 triggers *Glut1* transcription and augments glycolysis. Thus, ATF4 exerts bilateral effects on metabolic regulation. On the one hand, ATF4 suppresses mitochondrial oxidative metabolism through inhibition of TFAM activity and, on the other hand, ATF4 boosts glycolysis by activating *Glut1* expression. The detailed working model of LONP1-mediated mitochondrial quality control in safeguarding metabolic shifts is presented in Fig. 9.

From this study, two important conclusions could be drawn: (1) mitochondrial quality control is essential for heart development; and (2) mitochondrial quality control safeguards metabolic shifts during heart development. Thus, LONP1 connects mitochondrial quality control with metabolic shifts to ensure an energy supply for embryonic heart development.

MATERIALS AND METHODS

Mice

We used *Lonp1*-floxed, *Mef2c-AHF-Cre*, *cTnT-Cre*, *ctTA-Cre* and *ERt2-Cre* mice (from The Jackson Laboratory, Stock no: 008463) in this study. All mouse strains were maintained on a C57BL/6 genetic background. Mice were group-housed in accordance with the regulations on mouse welfare and ethics of Nanjing University, with 12 h/12 h light–dark cycles and *ad libitum* access to food and water. The Institutional Animal Care and Use Committee (IACUC) of the Model Animal Research Center of Nanjing University approved all animal procedures used in this study.

IF staining

Embryos and hearts fixed in 4% paraformaldehyde (PFA) were dehydrated and embedded in paraffin. Eight-micrometer-thick sections were cut using a Leica RM2016 microtome and then deparaffinized in xylene. Decreasing concentrations of ethanol were used to rehydrate the sections, which were then stained with Hematoxylin and Eosin (H&E; Uteambio, H0006-5G; SHJ0594).

Embryos and hearts fixed in 4% PFA were dehydrated and embedded in OCT medium (Sukura, 4583). Eight-micrometer-thick sections were cut using a Leica CM1950 automated cryostat. For IF staining, sections were placed at room temperature for 20 min and washed in PBS; goat serum

Development (2022) 149, dev200458. doi:10.1242/dev.200458

(Beyotime, C0265) was used to block the sections, which were then incubated with primary antibodies overnight at 4°C. The next day, the sections were washed with PBS and incubated with secondary antibodies for 2 h. DAPI stains the nuclei. Finally, the sections were washed again in PBS and sealed with 50% glycerol before confocal imaging. Details of the antibodies used are shown in Table S1.

Following a previously described protocol (Vaccaro et al., 2020), *in situ* ROS detection was performed using 2′,7′-dichlorofluorescein (H2DCF; Invitrogen, D399) in fresh E11.5 hearts. Briefly, fresh hearts were washed with PBS and then immediately incubated in the dark with 10 µM H2DCF and DAPI for 15 min at room temperature. Before mounting, tissues were washed with PBS three times for 5 min each time.

Isolation and culture of primary cardiomyocytes and MEFs

Lonp1$^{F/F}$ and *cTnT-Cre; Lonp1*$^{F/F}$ primary cardiomyocytes were derived from E13.5 hearts. Under aseptic manipulation, each heart was washed in cold PBS three times. The hearts were then digested using enzyme buffer [0.1% trypsin (Biochannel, BC-CE-006) and 0.25% collagenase type II (Gibco, 17101015)] concomitant with shaking at 37°C in a water bath. Digestion was stopped by adding fetal bovine serum (FBS; Gibco, 10099) every 10 min and pipetting the solution. The operation was repeated until no obvious heart tissue was seen. The collected solution was centrifuged at 1000 ***g*** for 5 min, and 1 ml of complete medium (high-glucose Dulbecco's Modified Eagle Medium; Gibco, 12800017) was added, followed by transfer to a 6 cm Petri dish. After 2-3 h, nonadherent cardiomyocytes were transferred to new 6 cm Petri dishes. The cultured cardiomyocytes were used to perform IF staining, as described above.

Lonp1$^{F/F}$ and *ERt2-Cre; Lonp1*$^{F/F}$ MEFs were derived from E13.5 embryos. After removing the head, limbs and internal organs, the remaining tissues were washed with ice-cold PBS, digested with 1 ml 0.25% trypsin and cut into pieces using microscissors. After digestion at 37°C for 15 min in a 6 cm Petri dish, the cells were blown with pipette to disperse them, and then complete medium was added in addition to 0.5 mM 4-OH-tamoxifen (Sigma-Aldrich, H7904) to induce Cre expression over the following 3 days. The cells were then collected for western blot, quantitative real-time PCR and measurement of mtDNA copy number.

Cell culture and treatment assays

Adherent cells were cultured in complete medium (high-glucose Dulbecco's Modified Eagle Medium; Gibco, 12800017) supplemented with 10% FBS (Excell, FSP500) and 100 U/ml penicillin-streptomycin (Gibco, 15140122) at 37°C and 5% CO_2.

For RNAi, a small interfering RNA (siRNA) duplex, shown below, was designed to knockdown *Lonp1*. *siLonp1*-1: sense, 5′-GGGACAUCAU-UGCCUUGAATT-3′; antisense, 5′-UUCAAG-GCAAUGAUGUCCCTT-3′; *siLonp1*-2: sense, 5′-CCGAGAACAAGAAGGACUUTT-3′; antisense, 5′-AAGUCCUUCUUGUUCUCGGTT-3′. Mixed *siLonp1* was used to treat cells to achieve higher knockdown efficiency. According to the protocol, transfection was performed using GP-Transfect mate (Gene-Pharma, G04009). Cells were harvested for western blot and quantitative real-time PCR analysis.

For overexpression, different plasmids were constructed and transfected into 293T cells using Lipo2000 (Invitrogen, 11668019) according to the manufacturer's protocol. The primers used are detailed in Table S3. Cells were collected for western blot, quantitative real-time PCR and measurement of mtDNA copy number. For CDDO treatment, cells cultured normally to 80% density were supplemented with CDDO. The concentration of CDDO and the time of treatment varied depending on the experimental requirements (optimal working concentration and time course). Cells were harvested for western blot and quantitative real-time PCR analysis.

Western blot

The harvested heart tissues and cells were washed with PBS and then lysed on ice with RIPA buffer (Beyotime Biotechnology, P0013B) with a protease inhibitor cocktail (Roche, 4693116001) and PhosSTOP (Roche, 4906837001) for 30 min. The solution was then centrifuged at 13,500 ***g*** at 4°C for 15 min. Subsequently, the protein concentration in the collected supernatant was quantified by a BCA Protein Assay Kit (Beyotime, P0012). Proteins were isolated on SDS-PAGE gels (10%) and then transferred onto PVDF membranes (Millipore, IPVH00010). The proteins were then blocked with 5% bovine serum albumin (BSA; BioFroxx, 4240GR100) in Tris-buffered saline-Tween 20 (TBST; CST, 9997) and then incubated with different antibodies (Table S1). Given the small size of the embryonic hearts, two to six hearts were used per group, and the PVDF membranes were cut so that each section could be incubated with different antibodies to make optimal use of the samples available. All quantifications were performed by ImageJ.

Quantitative real-time PCR

Total RNA was extracted from the cardiac ventricles of (without atria and outflow tract) control, *cTnT-Cre; Lonp1*$^{F/F}$ and *Mef2C-AHF-Cre; Lonp1*$^{F/F}$ hearts and different cell lines by using TRIzol reagent (Invitrogen, 15596026). RNA reverse transcription was performed using a HiScript II Q Select RT Supermix for qPCR (+gDNA wiper) kit (Vazyme Biotech, R223-01). cDNA was used to generate a MicroAmp Optical 96-Well Reaction Plate (Applied Biosystems, N8010560) using an AceQ Universal SYBR Master Mix Kit (Vazyme Biotech, Q511-02) and an Applied Biosystems QuantStudio 5 Real-Time PCR System. Data were processed using the ΔΔCt analytical method with controls normalized to 1 to reveal the fold up- or downregulation. The primers used are detailed in Table S2.

mtDNA copy number assays

The mtDNA copy number of different tissues and cells was measured as previously described (Quiros et al., 2014). Total DNA was extracted using a FastPure DNA Isolation Kit (Vazyme Biotech, DC112-01). RNase was added to ensure no RNA interference. The total DNA was added to a MicroAmp Optical 96-Well Reaction Plate using an AceQ Universal SYBR Master Mix Kit and an Applied Biosystems QuantStudio 5 Real-Time PCR System. Primers used are detailed in Table S2.

Luciferase reporter assays

The full-length fragment of the mouse ATF4 coding sequence (CDS) was cloned into the pCMV7.1-3×FLAG vector. Based on the results predicted by JASPAR (https://jaspar.genereg.net/), the ∼2 kb *Glut1* promoter fragment and an ∼2 kb *Tfam* promoter fragment were cloned into the pGL3-Basic Vector (Promega, E1751) to generate the *Glut1*-2K Luc and *Tfam*-2K Luc vectors, respectively. The primers used are detailed in Table S3. Plasmids were transfected into cells using Lipo2000 (Invitrogen, 11668019). Luciferase reporter assays in 293T cells were performed using the Dual Luciferase Assay System (Promega, E1910) following a standard protocol (Jiang et al., 2021) after 24-36 h of transfection.

Statistical analysis

All data are reported as mean±s.e.m. Differences between mean values were compared by two-tailed unpaired Student's *t*-tests or one-way and two-way ANOVAs using GraphPad Prism 8.0 software. Differences were significant at $P < 0.05$.

Acknowledgements

We thank Dr Bin Zhou (Albert Einstein College of Medicine, New York) for providing the *cTnT-Cre* mice.

Competing interests

The authors declare no competing or financial interests.

Author contributions

Conceptualization: Z.Y., K.Z.; Methodology: K.Z., X.H., W.Z.; Formal analysis: K.Z.; Investigation: K.Z., X.H.; Resources: Z.Y., B.L.; Data curation: K.Z.; Writing - original draft: K.Z.; Writing - review & editing: Z.Y.; Supervision: Z.Y., W.Z.; Funding acquisition: Z.Y.

Funding

This work was supported by grants from the National Key Research and Development Program of China (2019YFA0801601) and grants from the National Natural Science Foundation of China (31930029, 91854111, 91954101 and 31771534) to Z.Y. and B.L.

Data availability

RNA-seq data has been uploaded to the SRA database with the accession number PRJNA800234.

Peer review history

The peer review history is available online at https://journals.biologists.com/dev/article-lookup/doi/10.1242/dev.200458

References

B'Chir, W., Maurin, A. C., Carraro, V., Averous, J., Jousse, C., Muranishi, Y., Parry, L., Stepien, G., Fafournoux, P. and Bruhat, A. (2013). The eIF2α/ATF4 pathway is essential for stress-induced autophagy gene expression. *Nucleic Acids Res.* **41**, 7683-7699. doi:10.1093/nar/gkt563

Bernstein, S. H., Venkatesh, S., Li, M., Lee, J., Lu, B., Hilchey, S. P., Morse, K. M., Metcalfe, H. M., Skalska, J., Andreeff, M. et al. (2012). The mitochondrial ATP-dependent Lon protease: a novel target in lymphoma death mediated by the synthetic triterpenoid CDDO and its derivatives. *Blood* **119**, 3321-3329. doi:10.1182/blood-2011-02-340075

Bruneau, B. G. (2020). The developing heart: from The Wizard of Oz to congenital heart disease. *Development* **147**, dev194233. doi:10.1242/dev.194233

Chen, S. H., Suzuki, C. K. and Wu, S. H. (2008). Thermodynamic characterization of specific interactions between the human Lon protease and G-quartet DNA. *Nucleic Acids Res.* **36**, 1273-1287. doi:10.1093/nar/gkm1140

Dara, L., Ji, C. and Kaplowitz, N. (2011). The contribution of endoplasmic reticulum stress to liver diseases. *Hepatology* **53**, 1752-1763. doi:10.1002/hep.24279

Fischer, F., Hamann, A. and Osiewacz, H. D. (2012). Mitochondrial quality control: an integrated network of pathways. *Trends Biochem. Sci.* **37**, 284-292. doi:10.1016/j.tibs.2012.02.004

Guimarães-Camboa, N., Stowe, J., Aneas, I., Sakabe, N., Cattaneo, P., Henderson, L., Kilberg, M. S., Johnson, R. S., Chen, J., McCulloch, A. D. et al. (2015). HIF1α represses cell stress pathways to allow proliferation of hypoxic fetal cardiomyocytes. *Dev. Cell* **33**, 507-521. doi:10.1016/j.devcel.2015.04.021

Harvey, R. P. (2002). Patterning the vertebrate heart. *Nat. Rev. Genet.* **3**, 544-556. doi:10.1038/nrg843

Jiang, M., Hu, H., Zhao, K., Di, R., Huang, X., Shi, Y., Yue, Y., Nie, J., Yu, S., Wang, W. et al. (2021). The G4 resolvase RHAU modulates mRNA translation and stability to sustain postnatal heart function and regeneration. *J. Biol. Chem.* **296**, 100080. doi:10.1074/jbc.RA120.014948

Jousse, C., Oyadomari, S., Novoa, I., Lu, P., Zhang, Y., Harding, H. P. and Ron, D. (2003). Inhibition of a constitutive translation initiation factor 2alpha phosphatase, CReP, promotes survival of stressed cells. *J. Cell Biol.* **163**, 767-775. doi:10.1083/jcb.200308075

Kao, T. Y., Chiu, Y. C., Fang, W. C., Cheng, C. W., Kuo, C. Y., Juan, H. F., Wu, S. H. and Lee, A. Y. (2015). Mitochondrial Lon regulates apoptosis through the association with Hsp60-mtHsp70 complex. *Cell Death Dis* **6**, e1642. doi:10.1038/cddis.2015.9

Kilberg, M. S., Shan, J. and Su, N. (2009). ATF4-dependent transcription mediates signaling of amino acid limitation. *Trends Endocrinol. Metab.* **20**, 436-443. doi:10.1016/j.tem.2009.05.008

Koyanagi, S., Hamdan, A. M., Horiguchi, M., Kusunose, N., Okamoto, A., Matsunaga, N. and Ohdo, S. (2011). cAMP-response element (CRE)-mediated transcription by activating transcription factor-4 (ATF4) is essential for circadian expression of the Period2 gene. *J. Biol. Chem.* **286**, 32416-32423. doi:10.1074/jbc.M111.258970

Lopaschuk, G. D. and Jaswal, J. S. (2010). Energy metabolic phenotype of the cardiomyocyte during development, differentiation, and postnatal maturation. *J. Cardiovasc. Pharmacol.* **56**, 130-140. doi:10.1097/FJC.0b013e3181e74a14

Lu, P. D., Harding, H. P. and Ron, D. (2004). Translation reinitiation at alternative open reading frames regulates gene expression in an integrated stress response. *J. Cell Biol.* **167**, 27-33. doi:10.1083/jcb.200408003

Lu, B., Lee, J., Nie, X., Li, M., Morozov, Y. I., Venkatesh, S., Bogenhagen, D. F., Temiakov, D. and Suzuki, C. K. (2013). Phosphorylation of human TFAM in mitochondria impairs DNA binding and promotes degradation by the AAA+ Lon protease. *Mol. Cell* **49**, 121-132. doi:10.1016/j.molcel.2012.10.023

Maroli, G. and Braun, T. (2021). The long and winding road of cardiomyocyte maturation. *Cardiovasc. Res.* **117**, 712-726. doi:10.1093/cvr/cvaa159

Matsushima, Y., Goto, Y. and Kaguni, L. S. (2010). Mitochondrial Lon protease regulates mitochondrial DNA copy number and transcription by selective degradation of mitochondrial transcription factor A (TFAM). *Proc. Natl. Acad. Sci. USA* **107**, 18410-18415. doi:10.1073/pnas.1008924107

Menendez-Montes, I., Escobar, B., Palacios, B., Gómez, M. J., Izquierdo-Garcia, J. L., Flores, L., Jiménez-Borreguero, L. J., Aragones, J., Ruiz-Cabello, J., Torres, M. et al. (2016). Myocardial VHL-HIF signaling controls an embryonic metabolic switch essential for cardiac maturation. *Dev. Cell* **39**, 724-739. doi:10.1016/j.devcel.2016.11.012

Olson, E. N. and Srivastava, D. (1996). Molecular pathways controlling heart development. *Science* **272**, 671-676. doi:10.1126/science.272.5262.671

Pakos-Zebrucka, K., Koryga, I., Mnich, K., Ljujic, M., Samali, A. and Gorman, A. M. (2016). The integrated stress response. *EMBO Rep.* **17**, 1374-1395. doi:10.15252/embr.201642195

Quiros, P. M., Espanol, Y., Acin-Perez, R., Rodriguez, F., Barcena, C., Watanabe, K., Calvo, E., Loureiro, M., Fernandez-Garcia, M. S., Fueyo, A. et al. (2014). ATP-dependent Lon protease controls tumor bioenergetics by reprogramming mitochondrial activity. *Cell Rep* **8**, 542-556. doi:10.1016/j.celrep.2014.06.018

Quirós, P. M., Prado, M. A., Zamboni, N., D'Amico, D., Williams, R. W., Finley, D., Gygi, S. P. and Auwerx, J. (2017). Multi-omics analysis identifies ATF4 as a key regulator of the mitochondrial stress response in mammals. *J. Cell Biol.* **216**, 2027-2045. doi:10.1083/jcb.201702058

Rugarli, E. I. and Langer, T. (2012). Mitochondrial quality control: a matter of life and death for neurons. *EMBO J.* **31**, 1336-1349. doi:10.1038/emboj.2012.38

Shin, C. S., Meng, S., Garbis, S. D., Moradian, A., Taylor, R. W., Sweredoski, M. J., Lomenick, B. and Chan, D. C. (2021). LONP1 and mtHSP70 cooperate to promote mitochondrial protein folding. *Nat. Commun.* **12**, 265. doi:10.1038/s41467-020-20597-z

Song, J., Herrmann, J. M. and Becker, T. (2021). Quality control of the mitochondrial proteome. *Nat. Rev. Mol. Cell Biol.* **22**, 54-70. doi:10.1038/s41580-020-00300-2

Suzuki, C. K., Suda, K., Wang, N. and Schatz, G. (1994). Requirement for the yeast gene LON in intramitochondrial proteolysis and maintenance of respiration. *Science* **264**, 273-276. doi:10.1126/science.8146662

Vaccaro, A., Kaplan Dor, Y., Nambara, K., Pollina, E. A., Lin, C., Greenberg, M. E. and Rogulja, D. (2020). Sleep loss can cause death through accumulation of reactive oxygen species in the gut. *Cell* **181**: 1307-1328. doi:10.1016/j.cell.2020.04.049

Vattem, K. M. and Wek, R. C. (2004). Reinitiation involving upstream ORFs regulates ATF4 mRNA translation in mammalian cells. *Proc. Natl. Acad. Sci. USA* **101**, 11269-11274. doi:10.1073/pnas.0400541101

Xu, M., Yao, J., Shi, Y., Yi, H., Zhao, W., Lin, X. and Yang, Z. (2021). The SRCAP chromatin remodeling complex promotes oxidative metabolism during prenatal heart development. *Development* **148**, dev199026. doi:10.1242/dev.199026

Zhao, Q., Sun, Q., Zhou, L., Liu, K. and Jiao, K. (2019). Complex regulation of mitochondrial function during cardiac development. *J. Am. Heart Assoc.* **8**, e012731. doi:10.1161/JAHA.119.012731

Zurita Rendon, O. and Shoubridge, E. A. (2018). LONP1 is required for maturation of a subset of mitochondrial proteins, and its loss elicits an integrated stress response. *Mol. Cell. Biol.* **38**, e00412-17. doi:10.1128/MCB.00412-17